Teaching Optics with a Spatial Light Modulator

Manuel P. Cagigal, Vidal F. Canales, Pedro J. Valle, José E. Oti, Daniel M. de Juana
Dpto. de Fisica Aplicada, Universidad de Cantabria, Los Castros S/N, Santander 39005, Spain

ABSTRACT

The appearance of commercial spatial light modulators (SLM) opens new ways for teaching some optical phenomena. There are possible applications in a great variety of fields: interferometry, diffraction theory, simulation and compensation of random media, Fourier Optics, etc. In this paper, we propose the use of low cost liquid crystals displays (LCDs) as SLMs to perform some interesting optical experiments. The liquid crystal SLMs are extracted from a commercial video projector. This is one of the cheapest ways to obtain a SLM. For phase modulation, it requires the calibration of the system, because the manufacturers do not provide the physical specifications of the LCDs. This work is quite instructive since many different aspects are involved in the calibration process. Finally, we show an experiment using this setup, which demonstrates that the proposed SLM is an easy-to-use and flexible tool to show some well-known optical phenomena.

Keywords: spatial light modulator, liquid crystal, diffractive optics, random media simulation.

1. INTRODUCTION

Spatial light modulators are useful for teaching some optical phenomena. The use of commercial liquid crystals displays as SLMs has two advantages: they can be used to perform some interesting optical experiments and they can be obtained from a video projector at low cost. Since a low cost SLM is not characterized by the manufacturer, the system must be calibrated if we desire to perform phase modulation. This process is presented in section 2. It is quite instructive since many different aspects are involved in the calibration process. Section 3 describes several possible applications to a great variety of fields:

- Interferometry: a Point-Diffraction interferometer or a Young's experiment can be built in a very simple and flexible way.
- Diffraction theory: many objects and shapes can be used. It can even be used to show the effect of some apodizing functions over the diffraction image, or to create Fresnel lenses.
- Fourier Optics: the use of SLM in Fourier optics is well known and it is a common tool for filtering and correlation.
- Simulation and compensation of inhomogeneous media: the SLM offers the possibility of simulating the behavior of inhomogeneous media as the atmosphere or biological tissues. It can also be used in an adaptive optics system to compensate the distortions introduced by these media.

In section 4 a particular application in which the SLM has been used is explained: the simulation and compensation of atmospheric turbulence. The results show that the SLM is an easy-to-use and flexible tool to show some well-known optical phenomena, with the additional advantage of presenting low cost.

2. CALIBRATION OF THE PHASE MODULATOR

Twisted-nematic liquid crystal televisions are used as intensity or phase modulators in a great variety of applications,[1-4] because they can be obtained relatively cheaply from commercial video projector units. Furthermore, these devices have greater resolution than other devices specifically designed to be used as phase modulators in scientific applications. In this paper they are used to simulate a partial compensation AO system.[5]

Their main drawbacks are that their switching speed is relatively slow, that it is not possible to have a perfect intensity-only or phase-only modulation, and, finally, that proper use of such displays requires knowledge of the physical parameters of the device, including the twist angle, the birefringence and the orientation of the director axis.[6] These

Seventh International Conference on Education and Training in Optics and Photonics,
Tuan-Kay Lim, Arthur H. Guenther, Editors, Proceedings of SPIE Vol. 4588 (2002)

drawbacks limit their use in certain scientific applications, but are not so important in educational environments. Hence we have carried out several experiments to obtain these parameters in the cells LCX012BLA extracted from a SONY VPL-V500QM projector. Features of the device include 640x480 pixels of 31.5x31.5 μm and separation between pixel centers 42 μm. They are explained in subsection 2.1.
Furthermore, once the parameters are known the cell phase and intensity modulation must be calibrated as a function of the applied voltage for different configurations of the system. This additional calibration is described in subsection 2.2.

2.1 Physical parameters

There are several techniques to obtain the system parameters.[2,7-9] We chose the former with some modifications[6,10,11] to avoid ambiguities in the determination of the parameters. The experimental procedure consists on the measurement of the cell transmission between polarizers (crossed $T_\perp$ and parallel $T_\parallel$) when no voltage is applied, as a function of the angle rotated simultaneously by the polarizers axis, ψ_1. This transmission is a function of the fundamental cell parameters:[2]

$$T_\perp \propto \left[\cos\chi\,\mathrm{sen}(\alpha)+\frac{\alpha}{\chi}\mathrm{sen}\,\chi\cos(\alpha)\right]^2+\left[\frac{\beta}{\chi}\mathrm{sen}\,\chi\,\mathrm{sen}(2\psi_1-2\psi_D-\alpha)\right]^2$$
$$T_\parallel \propto \left[\cos\chi\cos(\alpha)+\frac{\alpha}{\chi}\mathrm{sen}\,\chi\,\mathrm{sen}(\alpha)\right]^2+\left[\frac{\beta}{\chi}\mathrm{sen}\,\chi\cos(2\psi_1-2\psi_D-\alpha)\right]^2 \qquad (1)$$

where α is the twist angle, β the birefringence, ψ_D the orientation of the director axis and $\chi=\sqrt{\alpha^2+\beta^2}$. To find a unique set of parameters, both transmissions must be measured for four different wavelengths,[6] which are provided using a helium-neon laser (632 nm) and an argon laser (wavelengths of 458, 488 and 514 nm). A curve-fitting routine is then used to determine the unknown parameters from the experimental data. In figure 1 the experimental transmissions and the fitted curves of one of the cells are shown. It can be seen that there is a perfect agreement between the experimental data and the theoretical predictions.
A further experiment is still required to determine the twist sign. The transmission is recorded once again but the analyzer is not rotated. This produces the data shown in figure 2 for the same cell. The comparison between the fitted curves shows clearly the correct sign for the twist angle.
Finally a π/2 ambiguity in the extraordinary axis direction must be eliminated using a simple technique.[10] The cell is illuminated with linearly polarized light and the diffraction pattern is examined when the external voltage applied is changed. There are changes in the diffraction pattern when the voltage is modified only if the incident light is polarized along the extraordinary axis. The resultant physical parameters that we obtain for our devices are shown in table 1. It is worth noting that we have adopted the same coordinate system as that of Lu and Soutar.[2]

2.2 Intensity and phase modulation

Once the physical parameters are known the phase and intensity modulation must be calibrated as a function of the voltage for different configurations of the system (i.e. brightness and contrast in the projector menu, gray level range and polarizers positions). Thus the most appropriate configuration for our particular application can be chosen. For example, in the case of the turbulent atmosphere that we will analyze in section 3, phase-only modulation is desired, because the atmosphere is assumed at first approximation as a phase screen.
To measure the intensity modulation, the cell is set between polarizers. The axis of the first one is parallel to the cell axis, while the second one is perpendicular to both of them. The transmission is measured as a function of the voltage applied to the cell, for different values of the brightness and contrast. The light source is a diode-pumped solid state laser with λ=532 nm while the detection device Newport 818SL is used with a Newport 1815C power meter to obtain a greater dynamic range. Figure 3 shows the intensity modulation for the different configurations. It can be seen that there is very low modulation for a null contrast. The intensity modulation is a linear function of the gray level (applied voltage) for a medium contrast while for a maximum contrast it saturates for relatively low values of the gray level.
The last step is the phase modulation measurement. The experimental setup shown in figure 4 allows the interference between two beams that travel through different areas of the cell. The voltage that is applied to the first of them is constant while the second one is variable. The interference pattern is detected in a CCD camera Elbex 380, and is processed in a PC using a frame grabber Data Translation 2861. As the voltage that is applied to the second area

changes, the interference fringes are shifted. By measuring this shift the phase modulation is found. Figure 5 shows the result obtained for the best configuration. The analysis of figures 3 and 5 shows two relevant characteristics. The first one is that the operating modes produce coupled amplitude and phase modulation (because of twist). The second one is that the phase range is lower than 2π. Both characteristics of our devices limit the level of compensation that can be simulated, as we will see in the next sections.

3. APPLICATIONS OF THE SLM

Once the low cost SLM based on the LCDs extracted from a video projector has been calibrated, it can be useful for a variety of applications. In fact, it can be a tool both for teaching and research in any field that requires intensity or phase modulation of the wavefront. Its main advantage is that the modulation pattern can be very easily modified. In this section, some possible applications of the device are briefly described, while in section 4, one of this applications is developed in detail.

3.1 Point diffraction interferometer

The point diffraction interferometer (PDI) is basically a two-beam interferometer in which a reference beam is generated by the diffraction from a small pinhole in a semitransparent coating. Its simplicity makes it suitable for testing instruments.[12] The PDI is a common-path interferometer and has the usual advantages of this class: the fringes are very stable against vibration and a white-light source can be used. It is clear that the PDI can be easily generated with a LCD. Furthermore, the use of LCD has an additional advantage. In practice, the diffracting region is not a point but has a finite size. The amplitude of the wave depends on how much of the light in the image falls on this region and this varies with aberrations of the wave. To produce an interference pattern of high visibility the filter should attenuate the amplitude of the direct wave to match. This indicates the advantage of using the LCD: a filter of different transmittance can be used for each case. For this application, as for every one that just requires intensity modulation, the calibration process explained in section 2 is not necessary.
Of course, there are some limitations to use this device. The main one is that the diffracting region should not be much larger than the center of the Airy disk that the original wave would produce if it had no aberrations.

3.2 Young's experiment

Young' experiment was the earliest experimental arrangement for demonstrating the interference of light. It is a key experiment for the understanding of wave mechanics, light coherence, quantum theory, etc. In this setup, light from a monochromatic point source falls on two pinholes which are close together in a screen and equidistant from the source. The pinholes act as secondary monochromatic point sources which are in phase, and the beams from them are superposed in the region beyond the screen.[13] In this region an interference pattern is formed. The pinholes can be generated using the LCD pixels.

3.3 Diffraction masks

The LCD can create any kind of diffraction masks with the only limitation of the pixel size. Then, the number of experiments that can be carried out is enormous (in both Fresnel and Fraunhoffer regimes): due to the high resolution of the device, as an example, diffraction patterns can be obtained for different apertures shapes, different number of apertures, or several distances between apertures, etc. Then, the effect of the combination of apertures, or the consequences of a periodic configuration can be easily shown using the LCD. A relevant example is the Talbot effect, also referred to as self- or lensless-imaging, observed when a beam of light is reflected or transmitted through a periodic pattern.[14] Another example of particular interest consists on the demonstration of the diffracting effects of a phase-only mask.

3.4 Diffraction gratings

Diffraction gratings can be obviously created with the proposed light modulator. They have a huge number of applications. For instance, they can be used to perform indirect wavefront measurements, because gratings can introduce lateral shear. For this task, low-frequency square bar patterns having unit modulation are typically used. [15] These are called Ronchi gratings. They can be used in either a collimated or converging beam. Either way the transmitted beam is broken up into a number of diffracted orders. The angle between the orders depends on the grating spacing, which is easily adjusted in the LCD. A final lens both recollimates the orders and images a pupil. On an

observation screen placed downstream of this lens, a number of overlapping circles of light are seen. In the overlap areas, one can see lateral shear interference fringes.

3.5 Image formation

There is a large number of applications where the LCD can be used for imaging. The first example is apodization. Apodization can be useful for improving the resolving power of optical systems, which is commonly known as superresolution. [16] The filters permit to achieve a significant reduction of the central lobe width of the irradiance point spread function. It can be useful in applications as optical data storage or confocal scanning microscopy. To do this, masks with different size, gray level or distribution, can be generated with the LCD, depending on the requirements. On the other hand, in some cases it is interesting to decrease not the central lobe, but a different area of the diffraction pattern, as in the search for exoplanets.[17] This can be achieved using an apodized aperture with the correct parameters.
Another possibility is to obtain an optical system with variable focal length, using variable zonal plates. The LCD is used to block alternate zones in the LCD. Again the main advantage is the capability of changing the configuration of blocked and unblocked zones in a fast and easy way.

3.6 Fourier optics

The LCDs extracted from the video projector can also be a useful tool for all the aspects related to Fourier optics.[18,19] As an example, they can be used to demonstrate the basic operations of computation by light. The LCDs can generate inputs that can be added, subtracted, multiplied, divided, averaged or differentiated. Furthermore, optical signal processing can be performed using the LCDs as the filters required, both with coherent and incoherent light. In the first case, some of the techniques that can be carried out are decoding by Fourier transform, inverse filters, Wiener filters, matched filter or convolution filter. If we use incoherent light, then we can obtain a multiple pinhole camera (the time modulated device is also very interesting) low pass filter with randomly distributed small pupils or incoherent matched filter.

3.7 Holographic memories

A black and white pattern can be used as a means of recording the binary numbers of 0's and 1's. This application is useful because the density of information that can be recorded in a sheet of histograms is enormous, provided a mechanism for picking up a particular hologram is available.[19] The LCD can be a tool to create binary patterns of any kind (not just black and white patterns), for performing experiments on this kind of optical memories.

3.8 Simulation and compensation of random media

Both the random phase and intensity fluctuations induced by a random medium can be simulated using the device. Furthermore, it can compensate for this distortion. A total or partial compensation process can be carried out. The two steps, simulation and compensation can be performed using a single LCD or using two devices. This application is explained in detail in next section.

4. ADAPTIVE OPTICS SYSTEM EXPERIMENTAL SETUP

The low cost SLM based on the LCDs extracted from a video projector can be useful for a variety of applications. As an example, in this section an experimental setup designed to simulate the effect of the turbulent atmosphere and the adaptive optics system is described. Its scheme is shown in Figure 6. Its main components are the object, the LCD that introduces the effect of the atmosphere and the AO system, the telescope and the data acquisition system. They are explained in detail in the next subsections.

4.1 Object

The light source is a diode-pumped solid state laser GM32-1H which provides 2 mW at λ=532 nm. A constant output power is obtained, because the laser is fed by a HP 6224B source which maintains a stable voltage of 5 V and a stable current of 0.37 A. The light emitted by the laser is linearly polarized and the polarization axis can be modified by rotating a $\lambda/2$ plate. The point source, a pin hole of diameter 50 μm, is placed immediately after the plate, and at the focal plane of a collimating system (focal length $\approx$ 40 cm). Thus, a planar wave front emanates from the whole system.

4.2 Atmosphere and AO system

Next to the collimating system the cell is situated between polarizers, with the axis of the first polarizer parallel to the director axis. The physical description of the cells has already been done. A single phase screen represents the contributions of both the atmosphere and the AO system.[20] It allows us to compare in subsection 4.5 experimental and theoretical data in the same conditions and to achieve a wider range of atmospheric and compensation configurations.

The procedure we followed to generate wavefronts with different degrees of compensation is that proposed by Roddier,[21] which gives the structure function predicted by Kolmogorov theory.[20] The wavefront is decomposed into Zernike polynomials, which allows us to control the degree of correction by assigning only a value of zero to the coefficient of the corresponding corrected polynomial. Wavefronts are simulated by use of a thousand polynomials, and thus the main limitation to generate high order terms is the number of pixels in the conditions of subsection 4.5.

The array of phase values that compose this wavefront is introduced in the cell as an image. Hence, the planar wave front is distorted when it travels through this setup as if it had traveled through the turbulent atmosphere and had been corrected with an AO system. We consider that its coherence area is equal to the pixel area. Consequently the Fried parameter, r_0, is 42 μm. The setup includes a monitor and an optical bench with an auxiliary LCD where the phase screen (i.e. the distortion introduced in the wave front) can be checked.

4.3 Telescope

The telescope which forms the image of the distorted wave front is composed by a diaphragm, preceding a microscope objective lens. In astronomical telescopes the ratio between the aperture and the focal length is usually 1/11. To match this condition the aperture is 1.8 mm. Thus, the ratio between the aperture and the Fried parameter is D/r_0 = (1.8 mm) /(42 μm) ≅ 40, which would correspond, for example, to a Fried parameter of 10 cm in a 4 m telescope (usual values in astronomical observatories when working in the visible). To change this ratio, both D and r_0 could be modified.

4.4 Data acquisition system

A microscope lens is placed at the focal plane of the telescope. The image formed by the microscope is detected by a high efficiency camera Photometrics CH350 with a CCD S1003BP detector (grade 1). The quantum efficiency of this device is 80% approximately. The detector resolution is 1024x1024 pixels, whose size is 24 μm. It is liquid cooled, at 35ºC below zero, to decrease the dark current to 3.3 electrons pixel^{-1} seg^{-1}. The dynamic range is 16-bit at 40 kHz or 12 bits at 500 kHz. The camera is connected to a PC using a 32bit PCI card. Hence the images recorded by the CCD can be analyzed using adequate software.

4.5 Results

A theoretical model for the turbulent atmosphere predicts a Rician distribution for the light intensity statistics.[22] This distribution has already been checked by comparing with simulated values.[22,23] In this subsection the Rician distribution is compared with experimental data, obtained using the setup previously described. The case of D/r_0=40, will be analyzed, although we have checked the set up in a wide range of conditions.

A series of fifty partially compensated wave fronts is represented into the LCD, and the corresponding images are recorded. The correction degree is 150 corrected Zernike modes. We obtain the normalized histograms of the light intensity at the PSF core, and in three consecutive coronas around it. The first one is placed at the border of the Airy core, the second one at the first ring and the last one at the halo. Figure 7 shows these histograms. The Rician distribution, Eq. (4), is also shown, and it can be seen that there is a good agreement between the theoretical predictions and the experimental data. The slight deviations could be solved using a greater number of images in the series. It is worth noting that, as the distance from the PSF core increases, the distribution evolves from a Gaussian type function towards an exponential distribution, characteristic of speckle. This confirms that partially corrected images are composed by a bright core surrounded by a speckled halo.[20,24,25] The theoretical model, which provides the proper intensity statistics, allows the attainment of other variables of great interest, that can be compared with experimental data. A parameter commonly used to determine the image quality is the Strehl ratio. Figure 8 shows the Strehl ratio (SR) as a function of the correction degree. It is compared with the theoretical expression.[7] The SR increases as the correction degree increases, because the energy is redistributed from the speckled halo towards the PSF core. When the correction degree is high, experimental and theoretical data are very similar, while when the correction is low, the theoretical SR is lower than the experimental one. The Marechal approximation $SR \approx \exp(-\Delta_j)$, which is only applicable for high correction degrees, also fits well the experimental data. The SR behavior is caused by the limitations of the phase range that the LCD provides. From table 1 and figure 5 it can be deduced that the phase range is limited to an interval of approximately 180º. The device can not generate phases out of this interval. As the phase distribution is

Gaussian, with D/r_0=40 it means that the device can generate at least 80% of the phase values only up to 200 corrected modes. Then it is easy to explain figure 8. The greatest phases can not be properly represented, so that the experimental SR is higher than it should be. For a high correction degree this effect is unimportant, but for low compensation a large number of phase values can not be represented and the SR does not match the real compensation degree.
To avoid this problem, there are thicker LCDs (generally inside older projectors) which offer a greater phase range, at the cost of a much slower (and complex) operation. Nevertheless the qualitative behavior of the SR is correct. Furthermore it fits precisely the theoretically predicted radial evolution and the high compensation behavior, because the limitations of the device are not so relevant in these cases.
Finally, the intensity modulation is another error source to take into account.

5. CONCLUSIONS

We have developed an experimental setup to simulate the atmosphere and the AO system effects on a wave front. Its main component, the phase modulator, is a LCD extracted from a commercial video projector. We have carried out several experiments to obtain the physical parameters and the intensity and phase modulation of the LCD.
Once the device has been calibrated, we have obtained experimental histograms of the image light intensity. There is a good agreement between these histograms and the Rician distribution predicted by the theory. It confirms the model, previously checked with simulated data. We have also compared the Strehl ratio. Again there is a good agreement between the theoretical and experimental values, except in those special conditions in which the limitations of the LCD are relevant (functions evaluated near the core and low correction degree).

ACKNOWLEDGMENTS

The authors would like to thank the optics group at the Universidad Autonoma de Barcelona for their help with the phase modulator setup. This research was supported by Dirección General de Enseñanza Superior grant AYA2000-1565-C01.

REFERENCES

1. J.A. Davis, I. Moreno and P. Tsai, "Polarization eigenstates for twisted-nematic liquid-crystal displays", *Appl. Opt.* **37**, 937-945 (1998).
2. C. Soutar and K. Lu, "Determination of the physical properties of an arbitrary twisted-nematic liquid crystal cell", *Opt. Eng.* **33**, 2704-2712 (1994).
3. K. Lu and B. Saleh, "Theory and design of the liquid crystal TV as an optical spatial phase modulator", *Opt. Eng.* **29**, 240-246 (1990).
4. O. Lopez-Coronado, I. Moreno, J. Campos and M. J. Yzuel, "Full in situ characterization of spatial light modulators in an optical correlator. Filter adaptation", *J. Mod. Opt.* **45**, 2461-2468 (1998).
5. D.J. Cho, S.T. Thurman, J.T. Donner and G.M. Morris, "Characteristics of a 128x128 liquid crystal spatial light modulator for wave-front generation", *Opt. Lett.* **23**, 969-971 (1998).
6. J.A. Davis, D.B. Allison, K.G. D´Nelly, M.L. Wilson and I. Moreno, "Ambiguities in measuring the physical parameters for twisted-nematic liquid crystal spatial light modulators", *Opt. Eng.* **38**, 705-709 (1999).
7. L.G. Neto, D. Roberge and Y. Sheng, "Full range, continuous, complex modulation by the use of two coupled-mode liquid-crystal televisions", *App. Opt.* **35**, 4567-4576 (1996).
8. J.A. Coy, M. Zaldarriaga, D.F. Grosz and O.E. Martinez, "Characterization of a liquid crystal television as a programmable spatial light modulator", *Opt. Eng.* **35**, 15-19 (1996).
9. R. Giust and J.P. Goedgebuer, "Determination of the twist angle and the retardation properties of twisted nematic liquid crystal televisions by spectral measurements", *Opt. Eng.* **37**, 629-634 (1998).
10. J. A. Davis, P. Tsai, K. G. D'Nelly and I. Moreno, "Simple technique for determining the extraordinary axis direction for twisted nematic liquid crystal spatial light modulators", *Opt. Eng.* **38**, 929-932 (1999).
11. J.A. Davis, P. Tsai, D.M. Cottrell, T. Sonehara and J. Amako, "Transmission variations in liquid crystal spatial light modulators caused by interference and diffraction effects", *Opt. Eng.* **38**, 1051-1057 (1999).

12. R.N. Smartt and W.H. Steel, "Theory and application of Point-Diffraction Interferometers," *Japan J. Appl. Phys.* **14**, 351-356 (1975).
13. M. Born and E. Wolf, *Principles of optics*, Cambridge University Press, Cambridge (1999).
14. Masud Mansuripur, "The Talbot effect," *Optics and Photonics News* 42-47 (April 1997).
15. J.M. Geary, *Introduction to wavefront sensors*, SPIE Press, Washington (1995).
16. M. Martínez-Corral, P. Andrés, C. Zapata-Rodríguez and M. Kowalczyk, "Three dimensional superresolution by annular filters," *Opt. Comm.* **165**, 267-278 (1999).
17. J.R.P.Angel, A.Y.S. Cheng and N.J. Woolf, "A space telescope for infrared spectroscopy of Earth-like planets," *Nature* **322**, 341-343 (1986).
18. J.W. Goodman,*Introduction to Fourier Optics*, McGraw-Hill, San Francisco (1968).
19. K. Lizuka, *Engineering Optics*, Springer-Verlag, Berlin (1987).
20. M.P. Cagigal and V.F. Canales, "Generalized Fried parameter after adaptive optics partial wave-front compensation", *J.Opt. Soc. Am. A* **17**, 903-910 (2000).
21. N. Roddier, "Atmospheric wavefront simulation using Zernike polynomials", Opt. Eng. **29**, 1174-1180 (1990).
22. V.F. Canales and M.P. Cagigal, "Rician distribution to describe speckle statistics in adaptive optics", *App. Opt.* **38**, 766-771 (1999).
23. V.F. Canales and M.P. Cagigal, "Photon statistics in partially compensated wave fronts", *J.Opt. Soc. Am. A* **16**, 2550-2554 (1999).
24. F. Roddier and C. Roddier, "National Optical Astronomy Observatories (NOAO) Infrared Adaptive Optics Program II: modeling atmospheric effects in adaptive optics systems for astronomical telescopes" in *Proc.of SPIE*, L.D. Barr, Ed., **628**, 298-304 (1986).
25. F. Rigaut, G. Rousset, P. Kern, J.C. Fontanella, J.P. Gaffard, F. Merkle and P. Léna, "Adaptive optics on a 3.6-m telescope: results and performance", *Astron. Astrophys.* **250**, 280-290 (1991).

		Red cell	Green cell	Blue cell
α		- 91.6º	- 90.4º	- 90.5º
ψ_D		47.2º	47.2º	47.2º
β	458 nm	227º	226º	221º
	488 nm	207º	203º	201º
	514 nm	190º	188º	185º
	633 nm	146º	145º	142º

Table 1. Fundamental physical parameters of the LCDs extracted from the projector.

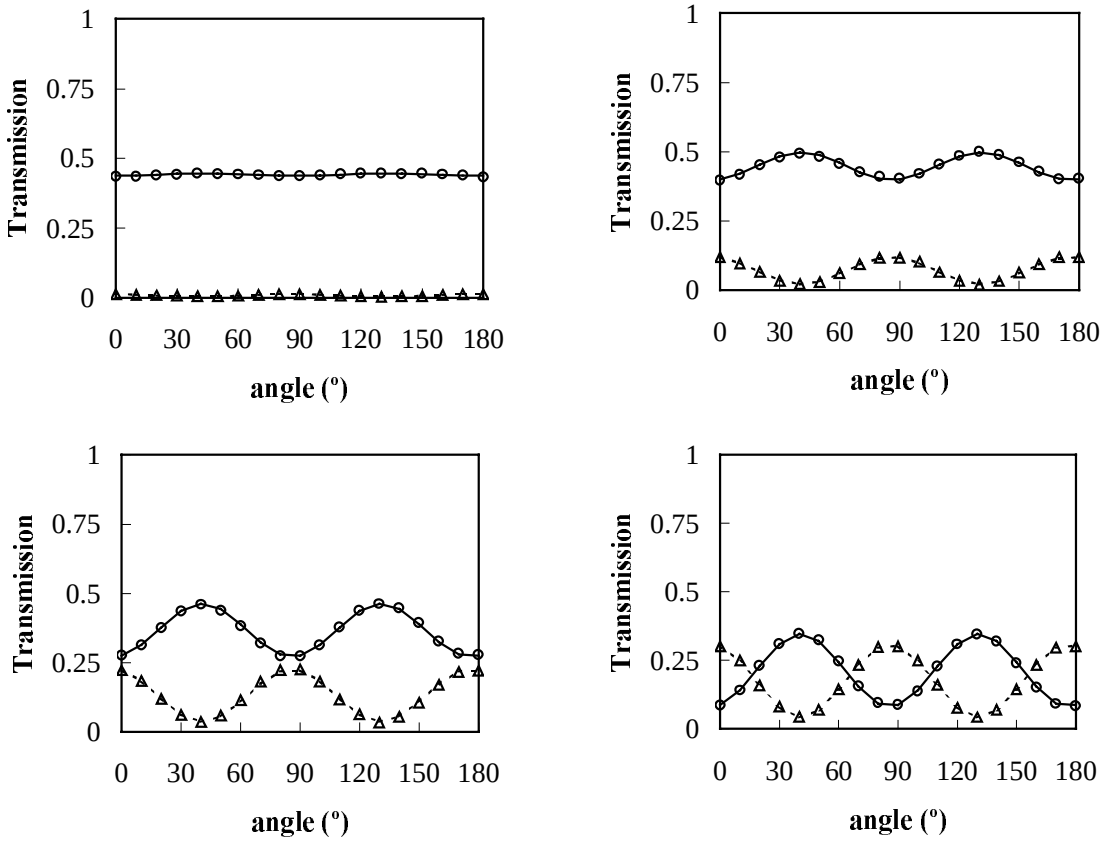

Figure 1 Red cell transmission as a function of the angle rotated by the polarizers. Crossed polarizers: theoretical prediction (solid curve) vs. experimental data (dots) and parallel polarizers: theoretical prediction (dashed curve) vs. experimental data (triangles). The graphs correspond to four different wavelengths, from left to right and from top to bottom: 633 nm, 514 nm, 488 nm and 458 nm .

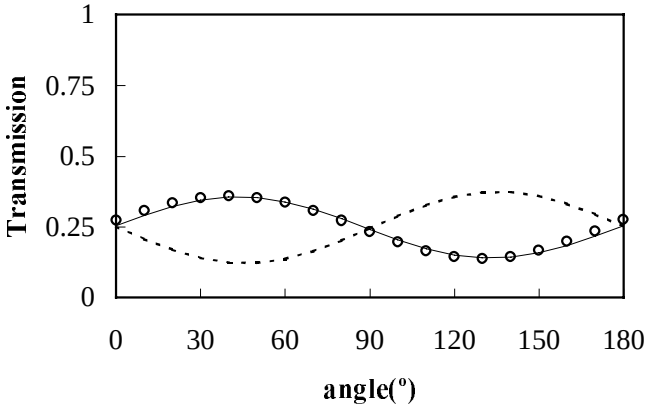

Figure 2 Transmission coefficient as a function of the angle rotated by the polarizer: experimental data (circles), theoretical curve with positive twist (dashed line) and with negative twist (solid line).

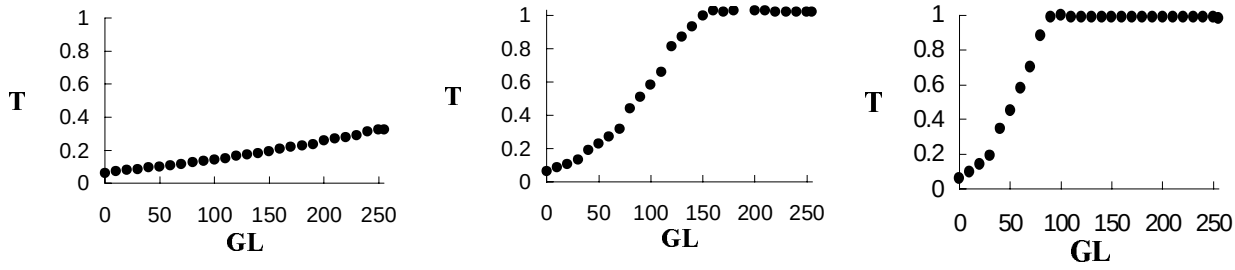

Figure 3 Transmission (T) as a function of the gray level (GL), for different configurations of the projector contrast (crossed polarizers and maximum brightness). The contrast is null in the first graph, the second one has intermediate contrast (50/100) and the last one, maximum contrast.

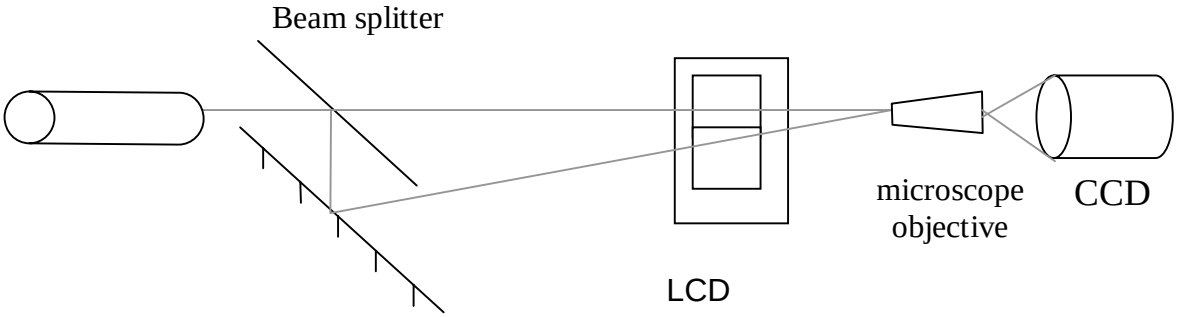

Figure 4 Experimental setup used to measure the phase modulation as a function of the gray level at the LCD.

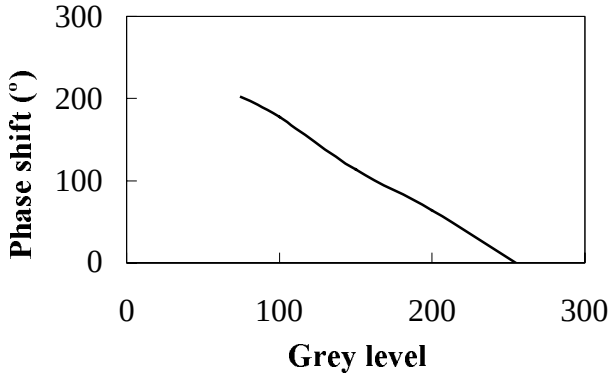

Figure 5 Phase modulation as a function of the gray level at the second area of the LCD (null brightness, intermediate contrast, parallel polarizers).

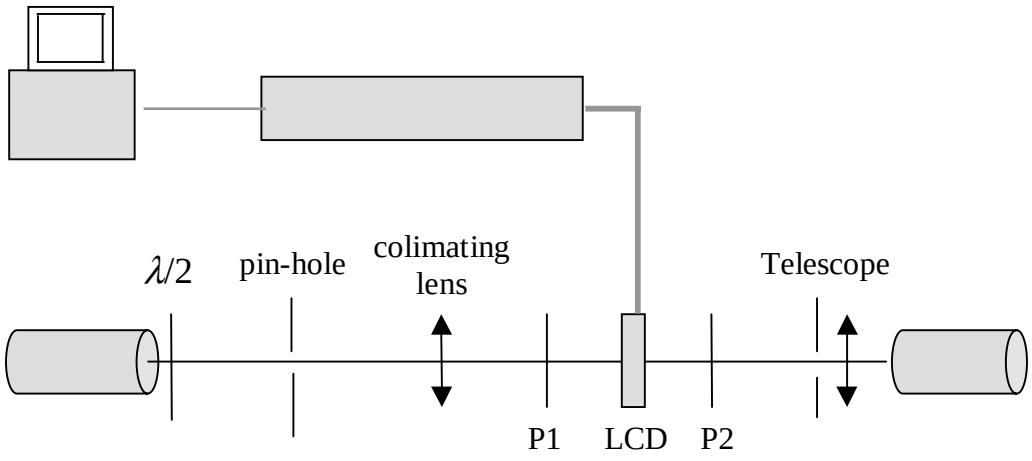

Figure 6 Experimental setup scheme which represents a telescope with an adaptive optics system.

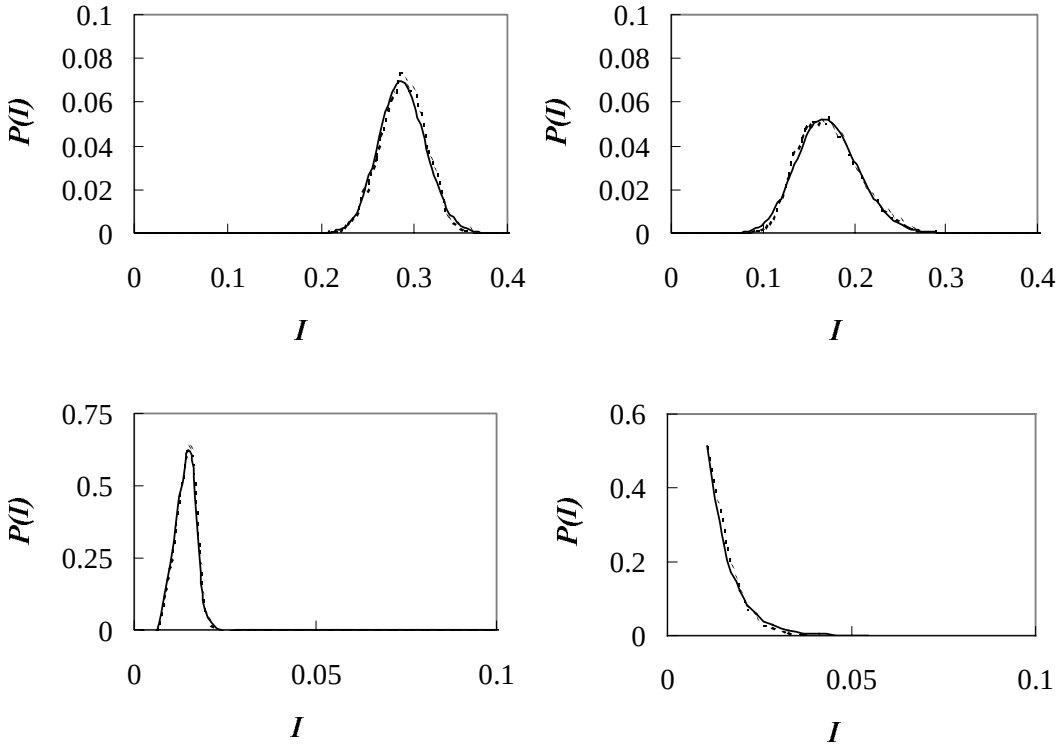

Figure 7 Normalized histograms of the light intensity (dashed line) at the image core (up left corner) and in three coronas around it. The first one (up right corner) is placed at the core border, the second (down left corner) at the first ring and the last one (down right corner) at the speckled halo, with D/r_0=40 and 150 compensated Zernike modes. They are compared with the Rice distribution (solid line).

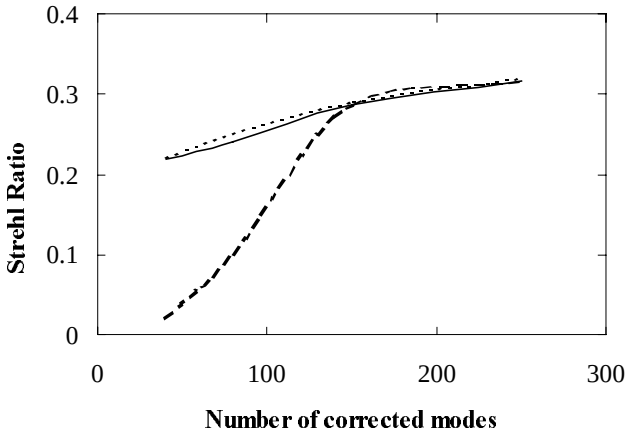

Figure 8 Comparison between the theoretical Strehl ratio (long dashed line) and the experimental value (short dashed line) as a function of the correction degree with D/r_0=40. Data corresponding to Marechal approximation are also shown (solid line).